

RESEARCH ARTICLE

One-step synthesis of magnetic-TiO₂-nanocomposites with high iron oxide-composing ratio for photocatalysis of rhodamine 6G

En Xie^{1,2,3}, Lei Zheng², Xinyang Li^{3,4}, Yingying Wang², Junfeng Dou², Aizhong Ding^{2*}, Dayi Zhang^{3,5*}

1 College of Water Resources and Civil Engineering, China Agricultural University, Beijing, PR China, **2** College of Water Sciences, Beijing Normal University, Beijing, PR China, **3** Lancaster Environment Centre, Lancaster University, Lancaster, United Kingdom, **4** School of Civil Engineering, Beijing Jiaotong University, Beijing, China, **5** School of Environment, Tsinghua University, Beijing, PR China

* zhangdayi@tsinghua.org.cn (DZ); ading@bnu.edu.cn (AD)



OPEN ACCESS

Citation: Xie E, Zheng L, Li X, Wang Y, Dou J, Ding A, et al. (2019) One-step synthesis of magnetic-TiO₂-nanocomposites with high iron oxide-composing ratio for photocatalysis of rhodamine 6G. PLoS ONE 14(8): e0221221. <https://doi.org/10.1371/journal.pone.0221221>

Editor: Bing Xu, Brandeis University, UNITED STATES

Received: May 14, 2019

Accepted: July 29, 2019

Published: August 19, 2019

Copyright: © 2019 Xie et al. This is an open access article distributed under the terms of the [Creative Commons Attribution License](https://creativecommons.org/licenses/by/4.0/), which permits unrestricted use, distribution, and reproduction in any medium, provided the original author and source are credited.

Data Availability Statement: All relevant data are available at [https://figshare.com/articles/One-step_synthesis_of_magnetic-TiO₂-nanocomposites_with_high_iron_oxide-composing_ratio_for_photocatalysis_of_rhodamine_6G/8397587](https://figshare.com/articles/One-step_synthesis_of_magnetic-TiO2-nanocomposites_with_high_iron_oxide-composing_ratio_for_photocatalysis_of_rhodamine_6G/8397587).

Funding: This project was funded by the National Natural Science Foundation of China (No. 51509003). DZ also acknowledges the support of Chinese Government's Thousand Talents Plan for Young Professionals. The funders had no role in

Abstract

In the study, a facile one-step method for synthesizing magnetic-TiO₂-nanophotocatalysts was developed. With the same composing ratio of 0.5 and 0.35 (Fe:Ti, mole:mole), we prepared two types of magnetic-TiO₂-nanocomposites as one-step synthesized Fe_xO_y-composed TiO₂ (Fe_xO_y/TiO₂-0.5 and Fe_xO_y/TiO₂-0.35) and two-step synthesized core-shell Fe_xO_y@TiO₂ (Fe_xO_y@TiO₂-0.5 and Fe_xO_y@TiO₂-0.35), and tested their performance in rhodamine 6G (R6G) photodegradation. X-ray diffraction (XRD) analysis showed that Fe_xO_y@TiO₂-0.5 has the smallest crystallite size (16.8 nm), followed by Fe_xO_y@TiO₂-0.5 (18.4 nm), Fe_xO_y/TiO₂-0.35 (21.0 nm) and Fe_xO_y/TiO₂-0.5 (19.0 nm), and X-ray photoelectron spectroscopy (XPS) suggested the decreasing percentage of Fe₃O₄ from 52.1% to 36.7%-47.2% after Ti-deposition treatment. The saturated magnetisms followed the order: Fe_xO_y@TiO₂-0.5 > Fe_xO_y@TiO₂-0.35 > Fe_xO_y/TiO₂-0.5 > Fe_xO_y/TiO₂-0.35. R6G photodegradation followed the first order kinetics and was slightly influenced by pH but significantly affected by initial photocatalyst concentration. Fe_xO_y/TiO₂-0.35 achieved the highest removal efficiency for R6G (92.5%), followed by Fe_xO_y@TiO₂-0.35 (88.97%), Fe_xO_y@TiO₂-0.5 (60.49%) and Fe_xO_y/TiO₂-0.5 (48.06%). Additionally, all these magnetic-TiO₂-nanocomposites had satisfied magnetic recoverability and exhibited laudable reusability after 5-times reuse, even achieving higher R6G removal efficiencies from 97.30% to 98.47%. Our one-step method took only 75 min for nanocomposite synthesis, 90 min less than conventional two-step method, showing its feasibility as a practical method for magnetic-TiO₂-nanocomposite synthesis in industrial application.

1. Introduction

Photocatalysis is one of most popular advanced oxidation processes (AOPs) in water treatment owing to its promising features of environment-friendly, generally non-selectivity and less

study design, data collection and analysis, decision to publish, or preparation of the manuscript.

Competing interests: The authors have declared that no competing interests exist.

secondary pollution [1]. In photocatalysis process, photocatalyst is the crucial component producing reactive oxygen species (ROS), *e.g.*, OH radicals [2], during the reaction by stopping recombination of photo excited electron hole pair on the surface of the photocatalysts [3]. Among them, titanium dioxide (TiO₂) is recognized as one of the best photocatalysts for its redox ability, high chemical and biological stability (particularly to photocorrosion), cost effectiveness and minor toxicity [3,4,5].

Bare TiO₂ photocatalysts have some inherent shortages. As working within a narrow ultra-violet wavelength [6], TiO₂ photocatalysts normally have a relatively low quantum efficiency and the most applied approach is minimizing the particulate size of TiO₂ to achieve a large specific surface area [7]. Accordingly, most TiO₂ catalysts are used in nano-scale [8,9], challenging the separation and recovery of these ultrafine particles after photocatalytic reaction. Considering their risks to the environment [10], recovering and reusing these TiO₂ nano-photocatalysts is of great urgency. To solve this problem, some approaches are developed to support TiO₂ nano-particulates with different anchors, *e.g.*, glass and ceramic [11]. Nevertheless, the photo-activities of these fixed-bed systems suffer from the low ratio of mass transfer, comparing to the suspension systems [4]. Recent studies therefore propose the introduction of iron elements in TiO₂ nano-photocatalysts as a promising method to achieve magnetic separation and harvesting [12]. Magnetic separation is more selective, efficient, and often much faster than centrifugation or filtration [13,14]. The key in magnetic separation is to generate strong magnetic forces on the target particles to overcome opposing forces, *e.g.* viscous drag, Brownian motion and sedimentation. Particulate size influences the magnetic forces [15], and decreasing the crystallite size from micrometers to nanometers significantly increases the magnetism by 100 to 1,000 times [16]. Thus, magnetic nanoparticulates (MNPs) have gained increasing attentions recently [17,18,19,20].

Coupling TiO₂ photocatalysts with MNPs provides a group of novel nanophotocatalysts integrating the superior photodegradation performance of TiO₂ and simple recovery by external magnetic fields. It has the potential to overcome the troubles in recovering and harvesting nanophotocatalysts after reuse. Generally, magnetic-TiO₂-nanophotocatalysts are manufactured by functionalizing the surface of MNPs with one thin layer of TiO₂ photocatalysts. Zhang *et al.* prepared magnetic-TiO₂-nanophotocatalysts via wrapping TiO₂ on montmorillonite and Fe₃O₄, achieving satisfied photodegradation rates and reusability for methylene blue [21]. Chen *et al.* synthesized three types of magnetic-TiO₂-nanophotocatalysts, showing that Fe₂O₃@TiO₂ had the highest adsorption efficiency (99%, 10 min) and Fe/TiO₂ achieved the highest photodegradation efficiency (94%, 150 min) for methylene blue [22]. Magnetic-TiO₂-nanophotocatalysts with different silver composing ratios could degrade 83.9% of methylene blue within 6 hours and the degradation efficiency remained 79% after 5-cycle reuse [23]. Although these magnetic-TiO₂-nanophotocatalysts achieved satisfied photodegradation efficiencies and magnetic recoveries, they all require a complicated multiple-step synthesis and time-consuming pre-synthesis of MNPs or TiO₂ precursor [5]. Alternatively, iron-composing is also used in TiO₂ nanophotocatalysts to modify the bandgap energy of TiO₂ and obtain a better photoactivity or extend the absorption spectrum [24,25]. The composing ratio of iron is normally less than 1% (mass ratio) owing to the declined photoactivity by excessive composing, and their magnetic recovery performance is not satisfied [26,27,28,29].

To the best of our knowledge, no previous research has reported simple or one-step synthesis processes to obtain iron-composed magnetic TiO₂ nanophotocatalysts with high Fe atomic percentage (>20%) via coprecipitation method. In this study, we developed a facile approach to synthesize magnetic-TiO₂-nanocomposites via one-step coprecipitation from iron and titanium salts. The synthesized magnetic-TiO₂-nanocomposites achieved comparable photocatalytic degradation performance of rhodamine 6G (R6G) and had good durability after recovery

and reuse. The main advantages of this method are: 1) simplified synthesis procedure without the need of pre-synthesizing MNPs or TiO₂ precursor; 2) 55% less synthesis time comparing to two-step method; 3) cost-saving for fewer reagents in synthesis process.

2. Materials methods

2.1 Magnetic TiO₂ synthesis

All the chemicals used in this study were of analytical grade and purchased from Sigma Aldrich (UK). One-step synthesis of TiO₂-composing MNPs followed the previously reported coprecipitation method with modifications [30,31]. Briefly, 2 mL FeCl₃ (1.0 M) and 1 mL FeCl₂ (2.0 M) were gently mixed and added with 20 mL titanium isopropoxide (TTIP, 97%) and isopropanol (IPA, ≥99.7%). The mixture was kept shaking, to avoid agglomeration, with drop-by-drop addition of 45 mL NaOH (1.0 M) to control the crystallization rate, and continuously homologized for 30 min by ultrasound (60 kHz, LNGF175, Langford Electronics Ltd., UK). The synthesized brown-dark nanoparticles were harvested by a permanent magnet and rinsed with ultrapure water until the supernatant reached neutral pH (7.0). To investigate the impacts of Fe-composing ratio, two TTIP-IPA mixtures (2.4:17.6 and 3.4:16.6, m:m) were used to synthesize magnetic-TiO₂-nanocomposites, named as Fe_xO_y/TiO₂-0.5 (Fe:Ti = 0.5, mole:mole) and Fe_xO_y/TiO₂-0.35 (Fe:Ti = 0.35, mole:mole). Details see [S1 Table](#).

In comparison, two TiO₂-coating magnetic nanophotocatalysts (core-shell), Fe_xO_y@TiO₂-0.5 (Fe:Ti = 0.5, mole:mole) and Fe_xO_y@TiO₂-0.35 (Fe:Ti = 0.35, mole:mole), were prepared using the conventional two-step synthesis method. Firstly, MNPs synthesis followed the reported protocol [32], except for Fe²⁺/Fe³⁺ ratio (1:1, mole:mole). The synthesized MNPs were washed with ultrapure water several times until pH was 7.0, and resuspended in 25 mL ultrapure water. Subsequently, 10 mL of MNPs suspensions were rinsed with 25 mL IPA three times for dehydration. Then, 25 mL IPA and 0.2 mL HCl (2.0 M) were added, gently mixed at 60 rpm, followed by rapidly adding TTIP of different volume (0.95 mL for Fe_xO_y@TiO₂-0.5 and 1.35 mL for Fe_xO_y@TiO₂-0.35) and keep shaking with drop-by-drop addition of 45 mL 1.0 M NaOH (at least 45 minutes). After ultrasonic treatment for 30 min, another 1 mL NaOH (1.0 M) was added with an extra one-hour ultrasonic treatment.

All the synthesized magnetic-TiO₂-nanocomposites were washed by ultrapure water until neutral pH. They were finally separated by magnet bar and dried overnight in a 60°C vacuum oven. After ground into powder, the granules were crystallized in a muffle furnace at 500°C for 4 hours.

2.2 Adsorption and photocatalysis experiment

Adsorption experiments were carried out in the dark to investigate R6G adsorption on magnetic-TiO₂-nanocomposites. R6G was dissolved in ultrapure water to make series concentrations from 1 to 25 mg/L. The synthesized magnetic-TiO₂-nanocomposites were added and the concentration was fixed as 0.4 g/L. The reaction system was kept continuous shaking (150 rpm) for 360 min and the water samples were collected at 1, 2, 3, 4, 5 and 6 hours. At each time point, the magnetic-TiO₂-nanocomposites were removed by external magnetic field and the supernatant was collected for R6G analysis. To test the effects of pH on R6G adsorption, R6G solution was adjusted to pH≈3, 7 and 10 by adding HCl (1.0 M) or NaOH (1.0 M), respectively.

R6G photodegradation was carried out in 6-well plates (Costar, UK), with a 20-watt UV lamp (253 nm) as the irradiation source. Initial R6G concentration was 10 mg/L, and the concentration of magnetic-TiO₂-nanocomposites was 0.4 g/L. During the 6-hour degradation experiment, the mixture was kept shaking at 150 rpm, and 250 μL of samples were collected at,

1, 2, 3, 4, 5 and 6 hours. After centrifugation at 10,000 rpm for 1 min, the supernatant was collected for R6G analysis. To test the effect of light wavelength on the photocatalytic degradation of R6G, 460-nm and 540-nm light was also used, following the same procedure described above. For the effects of pH and nanocomposite concentration on photocatalytic efficiency, the pH of the reaction system was adjusted to 3.0, 7.0 and 10.0 by adding HCl (1.0 M) or NaOH (1.0 M), and the concentrations of magnetic-TiO₂-nanocomposites were set as 0.2, 0.4 and 0.8 g/L. For each experiment, a blank control without UV light was set up and all the adsorption and photodegradation experiments were carried out in triplicates.

To test the durability of the synthesized magnetic-TiO₂-nanocomposites, they were recovered by a magnetic bar after 4-hour photodegradation of R6G, washed by ultrapure water for three times, dried at room temperature for 10 min, and finally added into fresh R6G for reuse, following the same procedure as described above. All the magnetic-TiO₂-nanocomposites were recovered and reused at least five times.

2.3 Chemical analysis

Fe and Ti oxidation phases of the synthesized magnetic-TiO₂-nanocomposites were analysed by X-ray photoelectron spectroscopy (XPS) via an ESCALAB 250Xi (Thermo Fisher, UK), using AlK α X-ray radiation ($h\nu = 1486.6$ eV, 1500 W) for excitation. X-ray diffraction (XRD) analysis was performed on an X'Pert PRO MPD diffractometer (PANalytical, Netherlands) equipped with Cu-K α radiation at 40 kV and 40 mA. Surface morphologies were analysed using transmission electron microscopy (TEM, Tecnai G2 F20, USA). A vibrating sample magnetometer (VSM, Lake Shore 7410, USA) was used to measure the magnetism of the synthesized magnetic-TiO₂-nanocomposites. Energy dispersive spectroscopy (EDS) analysis was conducted by a field emission scanning electron microscope (Quanta 450F, FEI, USA) with a voltage of 30 V. The Brunauer-Emmett-Teller (BET) surface area was measured by N₂ physisorption on an Autosorb iQ-C (Quantachrome Instruments, USA). The concentrations of MNPs and magnetic-TiO₂-nanocomposites were determined by gravimetric method. R6G concentration was determined by at 540 nm (excitation at 350 nm) by a multimode plate reader (FLUOstar Omega, Germany).

2.4 Data analysis

All the data were presented in terms of mean \pm standard deviation. The removal efficiency (%) of R6G was calculated by the equation $(C_0 - C_t)/C_0$, where C_0 is the initial concentration of R6G in the solution (mg/L) and C_t is the R6G concentration at time t (mg/L). Data of XPS and XRD were analysed by XPSpeak41 and Jade 6.5, respectively. The analysis of variance (ANOVA) was carried out via SPSS 20.0 for windows, and the significant level is $p < 0.05$.

R6G degradation or removal efficiency was calculated as the ratio of residual R6G to initial R6G in each treatment. The R6G degradation kinetics was calculated according to the first-order reaction, $\ln(C_t/C_0) = -k_{obs}t$. Here, k_{obs} is the photodegradation rate constant (h^{-1}). Both Langmuir and Freundlich isotherm models were used to assess the adsorption capacity of the synthesized magnetic-TiO₂-nanocomposites, as expressed in the following equations:

$$Q = Q_{max} \frac{K_L C}{1 + K_L C} \quad (1)$$

$$Q = K_F C^{1/n} \quad (2)$$

Here, Q is the amount of R6G adsorbed on magnetic-TiO₂-nanocomposites (mg/g), and C is the equilibrium concentration of R6G in aqueous phase (mg/L). For Langmuir isotherm,

Q_{max} is the theoretical maximum adsorption capacity (mg/g) and K_L is the adsorption equilibrium constant. K_F and n are the constants of Freundlich model.

To distinguish the different pathway of R6G loss by different magnetic-TiO₂-nanocomposites *via* adsorption, photolysis and photocatalysis, the changes of R6G concentrations in different treatments were calculated by Eqs (3) to (8).

$$\text{Total}_{0.2} = \text{PL}_{0.2} + \text{AD}_{0.2} + \text{PC}_{0.2} \tag{3}$$

$$\text{Total}_{0.4} = \text{PL}_{0.4} + \text{AD}_{0.4} + \text{PC}_{0.4} \tag{4}$$

$$\text{Total}_{0.8} = \text{PL}_{0.8} + \text{AD}_{0.8} + \text{PC}_{0.8} \tag{5}$$

$$PAD = \left(\frac{\text{AD}_{0.2}}{\text{Total}_{0.2}} + \frac{\text{AD}_{0.4}}{\text{Total}_{0.4}} + \frac{\text{AD}_{0.8}}{\text{Total}_{0.8}} \right) / 3 \tag{6}$$

$$PRL = \left(\frac{\text{PL}_{0.2}}{\text{Total}_{0.2}} + \frac{\text{PL}_{0.4}}{\text{Total}_{0.4}} + \frac{\text{PL}_{0.8}}{\text{Total}_{0.8}} \right) / 3 \tag{7}$$

$$PRC = \left(\frac{\text{PC}_{0.2}}{\text{Total}_{0.2}} + \frac{\text{PC}_{0.4}}{\text{Total}_{0.4}} + \frac{\text{PC}_{0.8}}{\text{Total}_{0.8}} \right) / 3 \tag{8}$$

Here, “0.2”, “0.4” and “0.8” indicates different treatments with initial magnetic-TiO₂-nanocomposites concentration of 0.2, 0.4 and 0.8 mg/L, respectively. AD is the R6G loss in treatments with magnetic-TiO₂-nanocomposites but no UV-irradiation. PL is the R6G loss in treatments with UV-irradiation but no magnetic-TiO₂-nanocomposites. Total is the R6G loss in treatments with both magnetic-TiO₂-nanocomposites and UV-irradiation. PC refers to the contribution of photocatalysis to R6G loss as calculated in Eqs (3)–(5). PAD, PRL and PRC refers to the average percentage of adsorption, photolysis and photocatalysis in R6G loss, respectively.

3. Results and discussion

3.1 Characteristics of magnetic-TiO₂-nanocomposites

After crystallization, all the four types of magnetic-TiO₂-nanocomposites had a red-brown colour (S1 Fig). TEM images (S2 Fig) illustrated that all the magnetic-TiO₂-nanocomposites had a typical solid particle structure, irregular ball or rod. Their crystallite size ranged from 10–100 nm, fitting well with the critical size suggested for effective magnetic separation (~50 nm) [16]. The morphologies of these particles were similar to that of Fe(III)-composed TiO₂ particles synthesized by previous work [33]. It is worth mentioning that the one-step synthesis of Fe_xO_y/TiO₂ nanocomposites took only 75 min, 55% less than that of Fe_xO_y@TiO₂ nanocomposites synthesized by conventional two-step method (165 min). EDS results (S3 Fig and S2 Table) showed different Fe/Ti ratios of synthesized magnetic-TiO₂-nanocomposites, which were 0.55 (Fe_xO_y/TiO₂-0.5), 0.34 (Fe_xO_y/TiO₂-0.35), 0.40 (Fe_xO_y@TiO₂-0.5) and 0.36 (Fe_xO_y@TiO₂-0.35), respectively, consistent with the theoretical data. The BET surface area of Fe_xO_y/TiO₂-0.5, Fe_xO_y/TiO₂-0.35, Fe_xO_y@TiO₂-0.5 and Fe_xO_y@TiO₂-0.35 was 2.9, 7.2, 42.1 and 31.3 m²/g, showing significant higher surface areas of Fe_xO_y@TiO₂ nanocomposites (two-step synthesis) than Fe_xO_y/TiO₂ nanocomposites (one-step synthesis).

Fig 1 shows the XRD patterns of MNPs and magnetic-TiO₂-nanocomposites. MNPs had sharp and intense peaks of magnetite (Joint Committee of Powder Diffraction Standard,

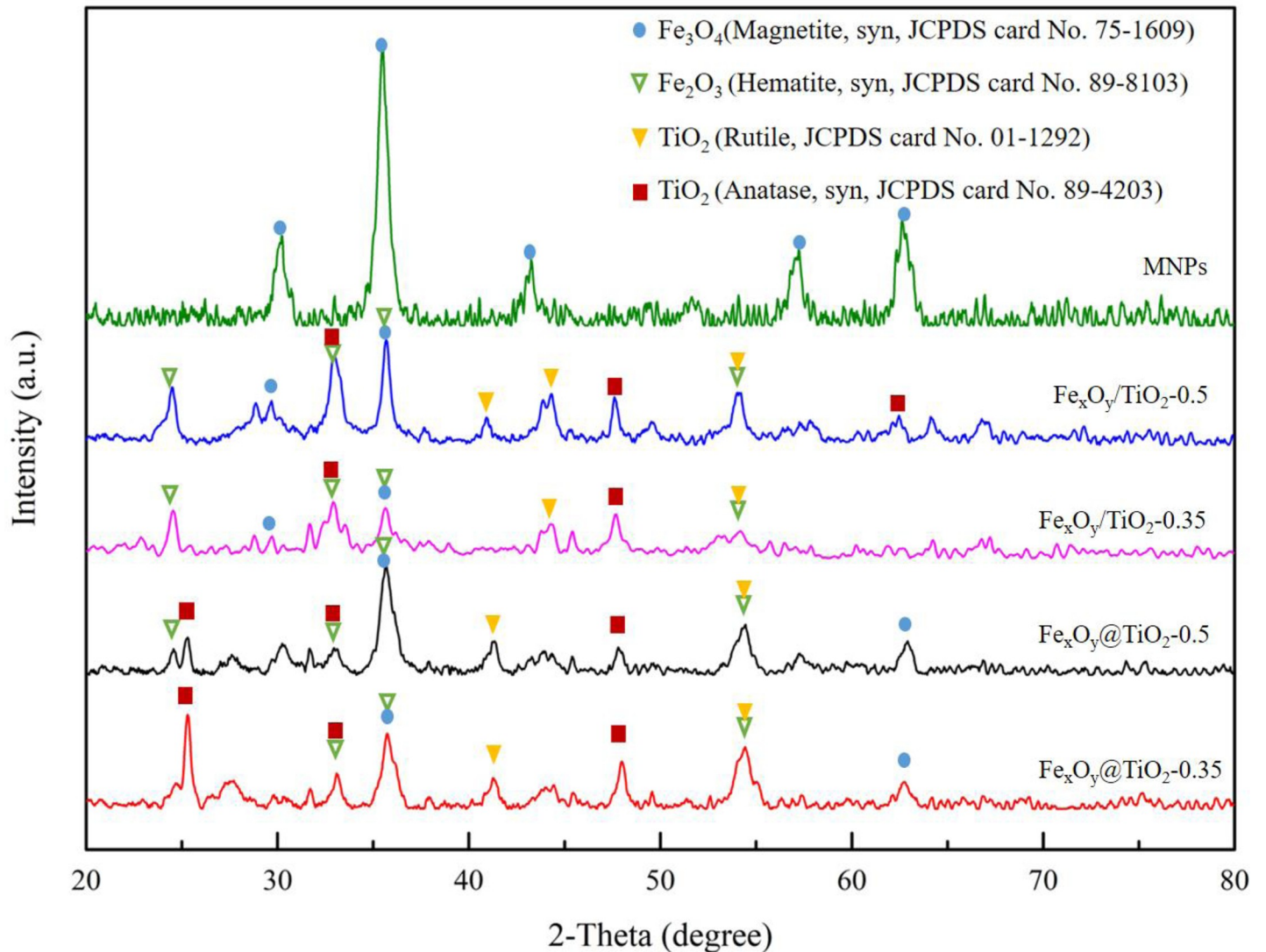


Fig 1. XRD patterns of MNPs and magnetic-TiO₂-nanocomposites. Characteristic peaks of magnetite, hematite, rutile TiO₂ and anatase TiO₂ are marked with blue circle, green triangle, yellow triangle and red square, respectively.

<https://doi.org/10.1371/journal.pone.0221221.g001>

JCPDS, card No. 75–1609), indicating its composition of an iron oxide Fe₃O₄. From Scherrer's formula [34], the average crystallite size of MNPs was 13.2 nm, calculated from the most intense peak corresponding to (311). For magnetic-TiO₂-nanocomposites, the peaks of TiO₂ were also observed at $2\theta = 25.30^\circ$ (101), 33.45° (110), 48.04° (200) and 62.68° (204) (Anatase, syn, card No. 89–4203), and at $2\theta = 27.51^\circ$ (110), 36.04° (101), 41.19° (111), 44.14° (210) and 54.23° (211) (Rutile, card No. 01–1292). It suggested the successful coupling of TiO₂ and MNPs, although there was some slight phase transformation presence in MNPs. The crystallite size of these magnetic TiO₂ was 19.0 nm (Fe_xO_y/TiO₂-0.5), 21.0 nm (Fe_xO_y/TiO₂-0.35), 18.4 nm (Fe_xO_y@TiO₂-0.5) and 16.8 nm (Fe_xO_y@TiO₂-0.35), all of which were larger than MNPs. It is worth noting that all the magnetic-TiO₂-nanocomposites had the signals of hematite (syn, card No. 89–8103) at the peaks $2\theta = 24.22^\circ$ (012) 33.24° (104), 35.74° (110), 54.22° (116) and 62.63° (214), suggesting the altered valence state of iron by titanium.

The elemental composition of the synthesized MNPs and magnetic-TiO₂-nanocomposites was analysed by XPS (Fig 2A). All the materials had iron and oxygen as core elements, owing to the main peaks of Fe 2p (710.3 to 710.7 eV) and O 1s (529.3 to 529.9 eV). One additional Ti 2p peak (457.8 to 457.9 eV) appeared in the XPS spectra of magnetic-TiO₂-nanocomposites. Fig 2B to 2F further show the Fe 2p bands in the binding energy region of 705–730 eV. MNPs showed the strongest intensity, followed by Fe_xO_y@TiO₂ nanocomposites. All the spectra of magnetic-TiO₂-nanocomposites could fit into two Fe 2p_{3/2} peaks (around 710 eV and 723 eV) and two Fe 2p_{1/2} peaks (around 711 eV and 725 eV) [35,36], suggesting the presence of both Fe₃O₄ and Fe₂O₃ [37]. Furthermore, the satellite peak at 719 eV is the main identity of Fe₂O₃ or FeO [38]. Accordingly, Fe₃O₄ accounted for 52.1% of the total iron oxides in MNPs, decreasing to 36.7%–47.2% in magnetic-TiO₂-nanocomposites. In addition, nanocomposites with higher Ti-deposition ratio had relatively higher proportion of Fe₂O₃, further proving the change of iron valence state by titanium.

The saturation magnetism (M_s) of Fe_xO_y/TiO₂-0.5, Fe_xO_y/TiO₂-0.35, Fe_xO_y@TiO₂-0.5 and Fe_xO_y@TiO₂-0.35 was 2.06, 1.40, 8.45 and 5.56 emu/g, respectively, as illustrated in Fig 2G. The coercivity (H_c) and remanence magnetization (M_r) of all the magnetic-TiO₂-nanocomposites were zero, indicating that the hysteresis loops were coincident completely and these nanocomposites dispersed well in the absence of external magnetic field. Generally, the saturation magnetisms of Fe_xO_y@TiO₂ nanocomposites were higher than Fe_xO_y/TiO₂ ones, explained by the incomplete coordination of iron atoms in the Fe_xO_y/TiO₂ nanocomposites [5]. Additionally, the saturation magnetism increased with the Fe/Ti ratio, owing to the strong link between M_s and the percentage of Fe₃O₄ [39]. The saturation magnetisms of our synthesized magnetic-TiO₂-nanocomposites fell in the range of previously studied magnetic nanophotocatalysts (0.54–42.2 emu/g, Table 1), indicating their comparable magnetic recovery or separation efficiency.

3.2 R6G adsorption isotherm

The adsorption of organic molecules on catalysts is an important process during photocatalysis [46], which is related to the R6G photocatalytic degradation efficiency by magnetic-TiO₂-nanocomposites. Our results indicated that all the magnetic-TiO₂-nanocomposites synthesized exhibited a significant R6G adsorption (S4 Fig). R6G aqueous concentrations decreased dramatically in the first 50 min and became stable in 1–2 hours. After 6-hour adsorption, Fe_xO_y@TiO₂-0.5 had the highest R6G adsorption capacity (1.65–18.62 mg/mg), followed by Fe_xO_y@TiO₂-0.35 (1.72–16.6 mg/mg), Fe_xO_y/TiO₂-0.5 (1.67–12.49 mg/mg) and Fe_xO_y/TiO₂-0.35 (1.75–8.61 mg/mg). Bare MNPs showed similar adsorption performance comparing to the synthesized magnetic-TiO₂-nanocomposites with no significant difference (data not shown, $p > 0.05$), indicating that the presence of Fe₃O₄ and Fe₂O₃ contributed to R6G adsorption but did not change the adsorption performance.

Fig 3 illustrates the satisfied fitness of the four magnetic-TiO₂-nanocomposites with Langmuir and Freundlich isotherms, respectively. From the isotherm parameters (Table 2), Langmuir adsorption described the adsorption mechanisms better except for Fe_xO_y/TiO₂-0.5 according to R^2 of each nanocomposite. Accordingly, Fe_xO_y@TiO₂ nanocomposites presented a better adsorption performance than Fe/Ti ones. Previous studies [47,48,49] suggested that the molecular adsorption on catalysts is involved in the surface complexation and ion exchange between the catalyst surface and the adsorbates. The functional groups located on the surface of TiO₂ include TiOH₂⁺, TiOH and TiO⁻ [50], which are more abundant than those on the surface of iron oxides [51]. The adsorption of R6G on nanocomposites is therefore dependent on the proportion of TiO₂ on the surface, which is higher in Fe_xO_y@TiO₂ nanocomposites.

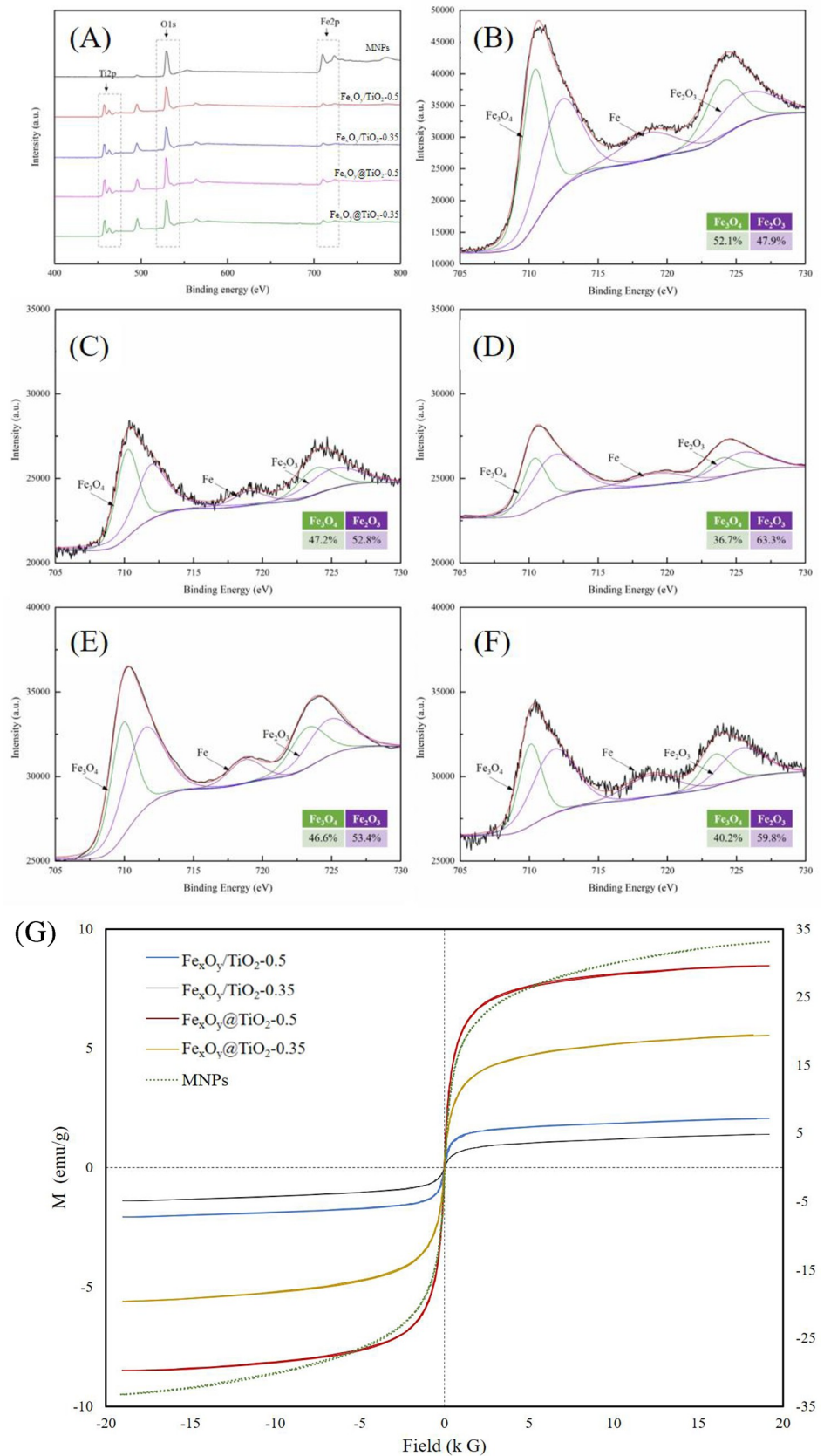
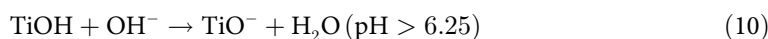
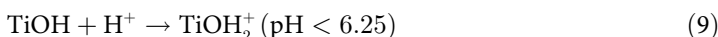


Fig 2. Characteristics of magnetic-TiO₂-nanocomposites. (A) XPS spectra of the synthesized MNPs and magnetic-TiO₂-nanocomposites. Fe2p region spectra: MNPs (B), Fe_xO_y/TiO₂-0.5 (C), Fe_xO_y/TiO₂-0.35 (D), Fe_xO_y@TiO₂-0.5 (E) and Fe_xO_y@TiO₂-0.35 (F). (G) Magnetization curve for magnetic-TiO₂-nanocomposites.

<https://doi.org/10.1371/journal.pone.0221221.g002>

In the present study, pH change from 3 to 10 did not significantly affect the R6G adsorption on magnetic-TiO₂-nanocomposites (S5 Fig, *p*>0.05). pH has been considered as one of the most important operational parameters in many photocatalytic systems, significantly affecting the photocatalytic efficiency *via* changing the structure and adsorption-desorption process of adsorbates. As the point of zero charge (PZC) for TiO₂ is 6.25 [5], the changes in surface charge of TiO₂ at various pH values are expressed in Eqs (9) and (10) [50]. At pH lower than PZC, the increasing proportion of TiOH₂⁺ led to the positively charged TiO₂ surface, whereas the negatively charged TiO⁻ occurs at pH>PZC. Meanwhile, R6G has a logarithmic acid dissociation constant (*pKa*) of 6.13, similar as the PZC for TiO₂. At pH>6.13, R6G is primarily in molecular state as the free electron pair on the primary amine group transfer to the aromatic rings and behave hydrophobic, but change to hydrophilic at lower pH when the protonation of nitrogen carries on in the secondary amine group of the xanthene ring [52]. Accordingly, the electrostatic force interactions between TiO₂ surface and R6G were reported to be weak repulsion or attraction in a broad range of pH [53], showing similar adsorption performance.



3.3 Contribution of adsorption, photolysis and photocatalysis to R6G degradation

Under all pH conditions, R6G exhibited limited removal without light (approximately 14.1%, S6 Fig) which was significantly lower than those with 253-nm UV-irradiation (averagely 73.58%, *p*<0.01, Fig 4). In addition, the R6G degradation efficiency with 460-nm or 540-nm irradiation (S7 Fig) was similar as that without light. It proved the significant contribution of photocatalysis to R6G degradation comparing to adsorption, and UV irradiation wavelength is a critical factor triggering R6G photodegradation with the aid of magnetic-TiO₂-nanocomposites. It is worth mentioning that there was neglectable R6G degradation in treatments with bare MNPs (data not shown), proving that neither Fe₃O₄ nor Fe₂O₃ contributed to R6G photocatalysis.

Table 1. Saturation magnetisms of reported magnetic nanophotocatalysts.

| Nanophotocatalyst | M _s (emu/g) | Reference |
|---|------------------------|-----------|
| Ce/TiO ₂ /NiFe ₂ O ₄ /diatomite | 6.8 | [40] |
| NiFe ₂ O ₄ /diatomite | 8.0 | [40] |
| Fe ₃ O ₄ /ZnO/Ag ₃ VO ₄ /AgI | 6.26 | [41] |
| Fe ₃ O ₄ /TiO ₂ | 7.5–42.2 | [42] |
| Fe ₃ O ₄ @SiO ₂ /TiO ₂ | 10.0–20.2 | [42] |
| Fe ₃ O ₄ @SiO ₂ @Iodine/TiO ₂ | 0.54–11.56 | [43] |
| Fe ₃ O ₄ @SiO ₂ @TiO ₂ | 15.9 | [44] |
| Fe ₃ O ₄ @SiO ₂ @TiO ₂ /Pd | 7.5 | [44] |
| Fe ₂ O ₃ -TiO ₂ | 0.55–2.14 | [45] |
| Fe _x O _y /TiO ₂ | 1.40–2.06 | This work |
| Fe _{3x} O _y @TiO ₂ | 5.56–8.45 | This work |

<https://doi.org/10.1371/journal.pone.0221221.t001>

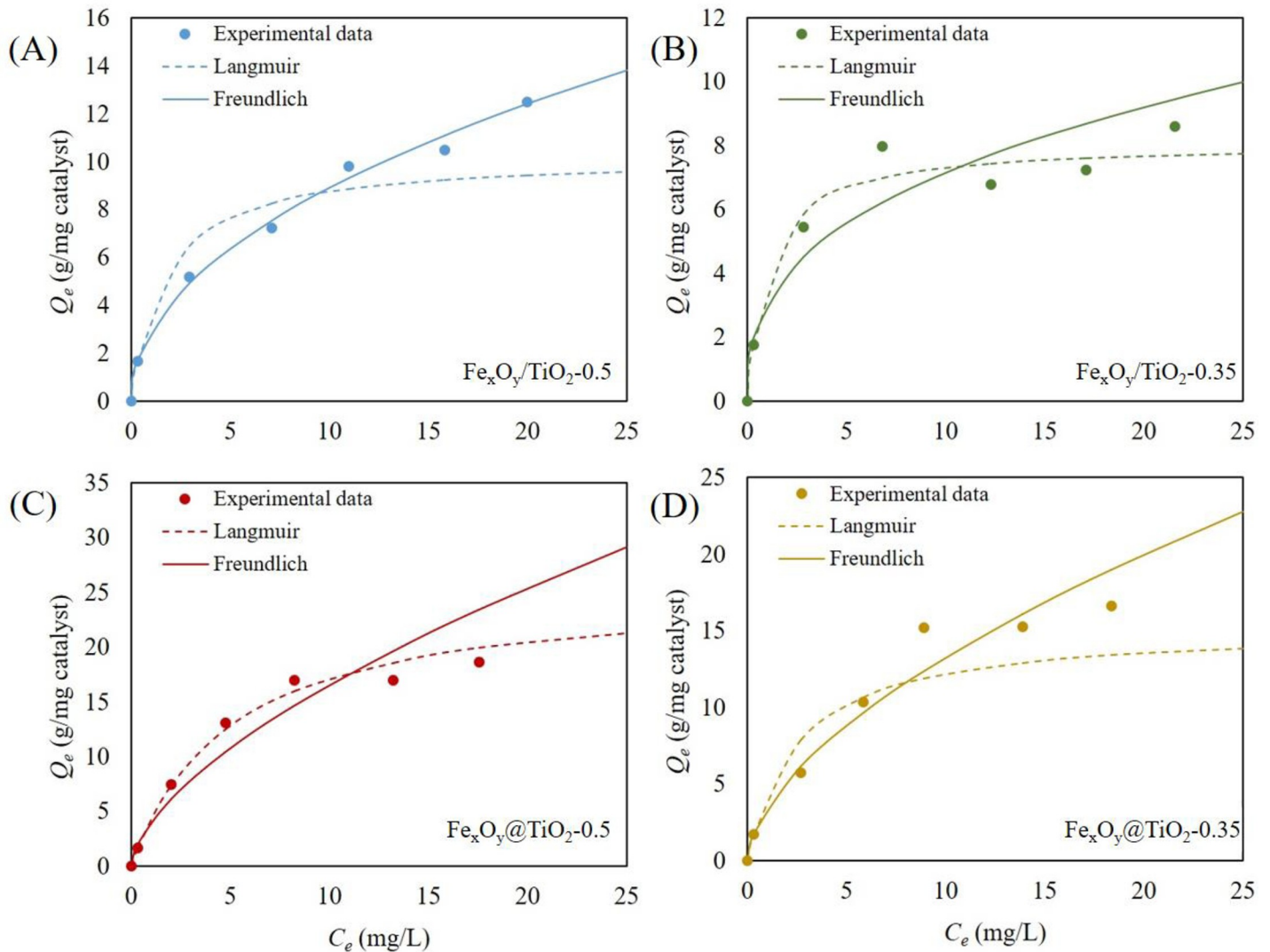


Fig 3. Langmuir (dotted line) and Freundlich (solid line) adsorption isotherms of R6G on the synthesized magnetic-TiO₂-nanocomposites. (A) Fe_xO_y/TiO₂-0.5, (B) Fe_xO_y/TiO₂-0.35, (C) Fe_xO_y@TiO₂-0.5, (D) Fe_xO_y@TiO₂-0.35. Dots represent experimental data. Experimental conditions: magnetic-TiO₂-nanocomposites concentration, 0.4 g/L; initial R6G concentration from 1 to 25 g/L; pH, 7.0.

<https://doi.org/10.1371/journal.pone.0221221.g003>

However, the loss of R6G might be explained by either adsorption, photolysis or photocatalysis as previously reported [46], which needs to be distinguished to evaluate the actual R6G photocatalysis performance.

Table 2. Parameters of Q_{max} and K_L in Langmuir isotherm and K_F and 1/n in Freundlich isotherm.

| Isotherm | Langmuir | | | Freundlich | | | |
|--|------------|-------------------------|----------------|----------------|-----------------------|--------|----------------|
| | Parameters | Q _{max} (mg/g) | K _L | R ² | K _F (mg/g) | 1/n | R ² |
| Fe _x O _y /TiO ₂ -0.5 | | 10.21 | 0.5883 | 0.9863 | 2.92 | 0.4831 | 0.9958 |
| Fe _x O _y /TiO ₂ -0.35 | | 8.09 | 0.9237 | 0.9943 | 3.10 | 0.3532 | 0.9036 |
| Fe _x O _y @TiO ₂ -0.5 | | 25.51 | 0.2030 | 0.9997 | 3.96 | 0.6204 | 0.9459 |
| Fe _x O _y @TiO ₂ -0.35 | | 15.29 | 0.3893 | 0.9862 | 3.41 | 0.5900 | 0.9816 |

<https://doi.org/10.1371/journal.pone.0221221.t002>

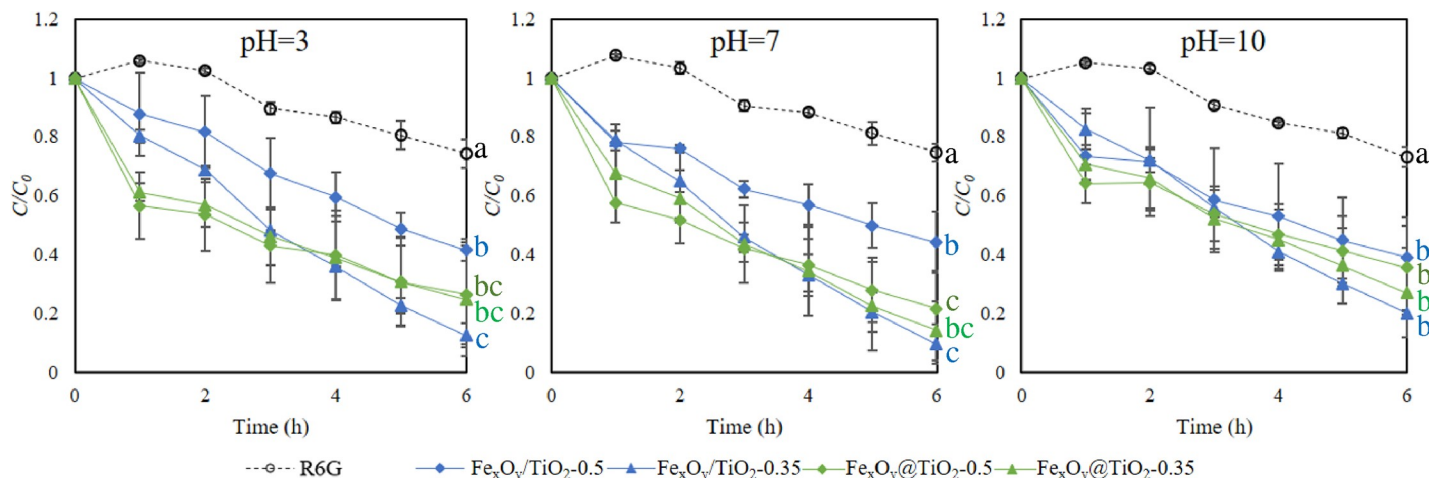


Fig 4. Impacts of pH on R6G photocatalysis performance. (A) pH = 3, (B) pH = 7, (C) pH = 10. Dotted lines represent the change of R6G concentration under UV-irradiation without magnetic-TiO₂-nanocomposites, and solid lines represent R6G photodegradation dynamics under UV-irradiation with magnetic-TiO₂-nanocomposites. Experimental conditions: UV-irradiation, 253 nm (20 W); magnetic-TiO₂-nanocomposites concentration, 0.4 g/L; initial R6G concentration, 10 mg/L. Different small letters after each line indicate significant difference (Duncan’s test, *p* < 0.05) among treatments (*n* = 3).

<https://doi.org/10.1371/journal.pone.0221221.g004>

S8 Fig summarizes the percentage of R6G loss during degradation, attributing to adsorption, photolysis and photocatalysis, respectively. Their contribution obviously varied across magnetic-TiO₂-nanocomposite types and concentrations. For instance, photolysis accounted for averagely 45.5% of the total R6G loss by Fe_xO_y/TiO₂-0.5, followed by adsorption (averagely 34.0%) and photocatalysis (averagely 20.5%). In contrast, photocatalysis had a higher contribution to R6G loss by Fe_xO_y@TiO₂-0.5 (averagely 31.3%). With the increasing TiO₂ proportion, the contribution of photocatalysis significantly increased to 58.3% for Fe_xO_y/TiO₂-0.35 and 63.1% for Fe_xO_y@TiO₂-0.35, which were close to Chen’s report (56.7%–67.1%) [23]. These results indicated that the photocatalytic performance of the synthesised magnetic-TiO₂-nanocomposites increased with the Ti/Fe ratio. Since the photocatalytic active sites are mainly located on TiO₂ instead of iron oxides [43], higher percentage of TiO₂ in magnetic-TiO₂-nanocomposites increases the photocatalysis capability. Iron-composing benefits the photocatalytic performance of TiO₂ because transition metal ions can act as shallow charge traps in the crystal structure, inhibiting the recombination of electron-hole pairs and prolonging their lifetime [54]. Although the impacts of transition metals on TiO₂ catalytic performance strongly depend on the composing ratio and are reported to peak at low level, all the previous studies focused on the low Fe-composing ratio, normally less than 10 at.% [33,55]. Our synthesised magnetic-TiO₂-nanocomposites had the high Fe:Ti ratio (Fe-atomic percentage ranging from 25.4–35.5%). For the first time, our results suggested magnetic-TiO₂-nanocomposites with high Fe-composing ratio still have satisfied photocatalysis capability.

3.4 Photocatalytic performance of magnetic-TiO₂-nanocomposites

R6G degradation curves in different treatments with the synthesised magnetic-TiO₂-nanocomposites are illustrated in Fig 4. In blank controls (no magnetic-TiO₂-nanocomposites), R6G concentration decreased only 25.6%, 25.2% and 26.9% under acidic (pH≈3), neutral (pH≈7) and basic (pH≈10) conditions after 6-hour experiment. In contrast, treatments with magnetic-TiO₂-nanocomposites achieved much higher removal efficiency, averagely 73.6% (pH≈3), 77.6% (pH≈7) and 69.5% (pH≈10), respectively. Especially, Fe/TiO₂-0.35 was the most efficient one (removal efficiency 85.9%), followed by Fe@TiO₂-0.35 (78.0%), Fe@TiO₂-0.5 (72.1%) and Fe/TiO₂-0.5 (58.3%).

Our results showed slightly higher R6G photodegradation efficiencies under neutral pH conditions than acidic and basic treatments. It might be explained by the higher R6G adsorption on magnetic-TiO₂-nanocomposites as mentioned above. As adsorption is a key step for photocatalysis [46], more R6G absorbed on magnetic-TiO₂-nanocomposites under neutral pH therefore contribute to higher R6G removal. A similar result was also reported that the highest efficiency was obtained at the neutral condition (pH = 7.4) during the phenol photodegradation process with TiO₂ as photocatalyst [50].

The impacts of magnetic-TiO₂-nanophotocatalyst concentration on R6G photocatalysis were investigated under neutral pH condition (pH ≈ 7), as shown in S9 Fig. For single kind of nanophotocatalyst, the initial concentration influence to R6G degradation significantly. For instance, the R6G removal efficiency in Fe_xO_y/TiO₂-0.5 treatment was 31.86% (0.2 g/L), 48.06% (0.4 g/L) and 39.09% (0.8 g/L), respectively (p < 0.05). It ranged from 74.63% to 92.50% for Fe_xO_y/TiO₂-0.35 (p < 0.05 except for 0.4 g/L vs. 0.8 g/L, p = 0.084), 40.72% to 60.49% for Fe_xO_y@TiO₂-0.5 (p < 0.05 except for 0.2 g/L vs. 0.4 g/L, p = 0.988) and 72.22% to 88.97% for Fe_xO_y@TiO₂-0.35 (p < 0.05). There was no significant difference in R6G removal efficiency between Fe/TiO₂ and Fe_xO_y@TiO₂ nanophotocatalysts (p = 0.329), hinting similar photocatalytic efficiency of magnetic-TiO₂-nanocomposites synthesized by one-step and two-step methods.

3.5 R6G photodegradation kinetics

The photocatalysis kinetics of R6G by different magnetic-TiO₂-nanocomposites are illustrated in Fig 5. R6G degradation followed the first-order kinetics (correlation coefficient above 0.9), consistent with previous study [52]. For two-step synthesized magnetic-TiO₂-nanocomposites, R6G photodegradation rate constant (k_{obs}) ranged from 0.0816 to 0.1351 h⁻¹ for Fe_xO_y@TiO₂-0.5, increasing to 0.1954–0.3454 h⁻¹ for nanophotocatalysts with higher Ti proportion (Fe_xO_y@TiO₂-0.35). They were similar with the degradation rate constant of one-step synthesized magnetic-TiO₂-nanophotocatalysts with no significant difference (p = 0.329), 0.0643–0.0939 h⁻¹ for Fe_xO_y/TiO₂-0.5 and 0.2225–0.4723 h⁻¹ for Fe_xO_y/TiO₂-0.35.

Among them, Fe_xO_y@TiO₂-0.35 and Fe_xO_y/TiO₂-0.35 nanocomposites showed higher photocatalytic activities than previously reported methylene blue degradation by magnetic-nanophotocatalyst Ni-Cu-Zn ferrite@SiO₂@TiO₂@Ag [23] (k_{obs} from 0.1326 to 0.2544 h⁻¹). It is worth noting that the dosage of magnetic-TiO₂-nanocomposites did not significantly change the k_{obs} , possibly attributing to the decrease of surface active sites as nanophotocatalysts aggregate at elevated concentration, or the declined light utilization efficiency caused by the increasing opacity level and scattering of light at high nanocomposite concentration [56].

3.6 Reusability of magnetic-TiO₂-nanophotocatalysts for R6G photodegradation

Reusability is a critical factor for evaluating the practical feasibility of nanophotocatalysts in industrial applications. After recycling the synthesized magnetic-TiO₂-nanocomposites and reusing them for R6G photocatalytic degradation five times, our results proved their satisfactory stability in photocatalysis, as illustrated in Fig 6. The photocatalytic activities of all the magnetic-TiO₂-nanocomposites remained unchanged or even increased in all the cycles. After 5 cycles, the R6G removal efficiency was up to 97.30% to 98.47%, and there was no significant difference between the four magnetic-TiO₂-nanocomposites. Additionally, R6G degradation still followed the first-order kinetics and the photodegradation rate constant k_{obs} was 0.1434–1.088 h⁻¹ (Fe_xO_y/TiO₂-0.5), 0.2380–1.1486 h⁻¹ (Fe_xO_y/TiO₂-0.35), 0.2554–0.9177 h⁻¹ (Fe_xO_y@TiO₂-0.5) and 0.3285–1.1411 h⁻¹ (Fe_xO_y@TiO₂-0.35), respectively. The increasing instead of

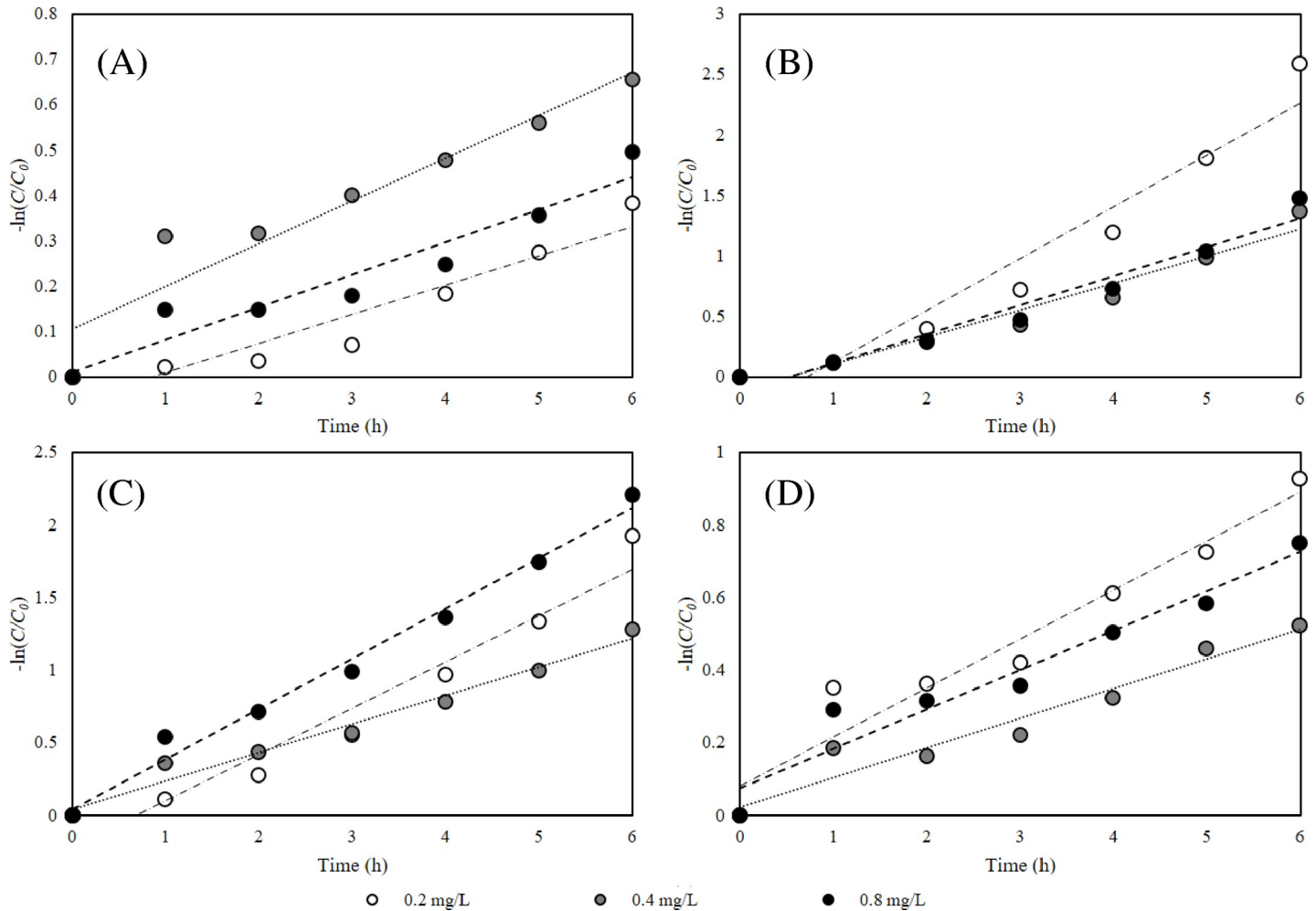


Fig 5. Impacts of initial magnetic-TiO₂-nanocomposite concentration on R6G photodegradation kinetics. (A) $\text{Fe}_x\text{O}_y/\text{TiO}_2-0.5$, (B) $\text{Fe}_x\text{O}_y/\text{TiO}_2-0.35$, (C) $\text{Fe}_x\text{O}_y@\text{TiO}_2-0.5$ and (D) $\text{Fe}_x\text{O}_y@\text{TiO}_2-0.35$. Experimental conditions: UV-irradiation, 253 nm (20 W); initial R6G concentration, 10 mg/L; initial magnetic-TiO₂-nanocomposites concentration, 0.2 mg/L, 0.4 mg/L and 0.8 mg/L, respectively; pH, 7.0.

<https://doi.org/10.1371/journal.pone.0221221.g005>

decreasing k_{obs} during reuse was also reported by some previous studied and might be explained by the activation of photocatalytic active sites [57,58,59].

Numerous studies have attempted to synthesize and reuse different types of magnetic nanophotocatalysts in removing dyes, as listed in Table 3. For industrial application, both photocatalytic capability and recovery ratio are important to achieve cost-effectiveness. Nevertheless, none of the studies mentioned above have provided data support. Here, we evaluated the recovery ratio for all the synthesized magnetic-TiO₂-nanocomposites, which were acceptable after 5-time reuse and achieved 68.83% for $\text{Fe}_x\text{O}_y/\text{TiO}_2-0.5$, 65.38% for $\text{Fe}_x\text{O}_y/\text{TiO}_2-0.35$, 80.32% for $\text{Fe}_x\text{O}_y@\text{TiO}_2-0.5$ and 77.84% for $\text{Fe}_x\text{O}_y@\text{TiO}_2-0.35$. Our result indicated long life-cycles of these synthesized magnetic-TiO₂-nanocomposites, and the recovery ratio might be further improved by increasing M_s to enhance magnetic separation efficiency and prolong their life-time.

Of all the concerns to apply nanophotocatalysts for industrial applications, including the extension of excitation wavelength, viability of magnetic separation, photocatalytic activity and cost-effectiveness in nanocomposite synthesis, our study attempted to reduce the synthesis

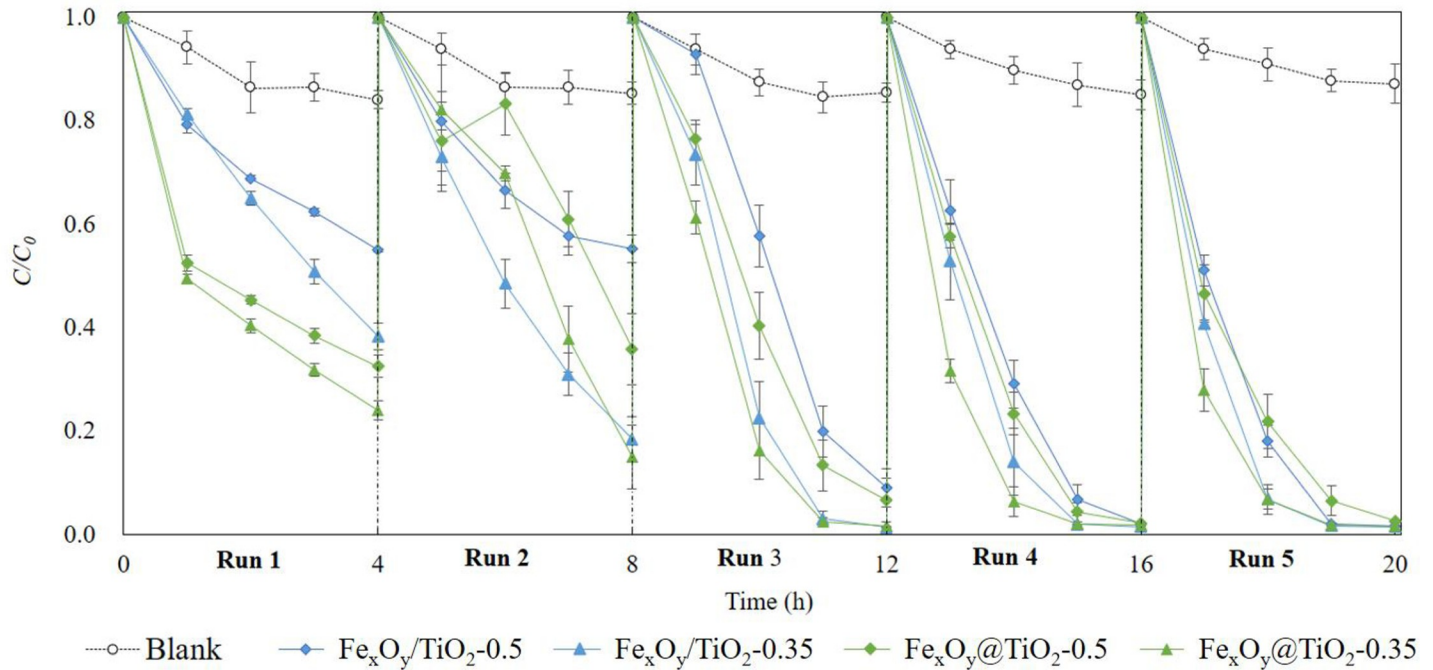


Fig 6. R6G degradation performance after reusing magnetic-TiO₂-nanocomposites 5 times. Dotted lines represent R6G concentration dynamics in blank treatment without magnetic-TiO₂-nanocomposites and solid lines represent R6G photodegradation dynamics under UV-irradiation with magnetic-TiO₂-nanocomposites. Experimental conditions: UV-irradiation, 253 nm (20 W); initial magnetic TiO₂ nanocomposites concentration, 0.4 g/L; initial R6G concentration, 10 mg/L; pH, 7.0.

<https://doi.org/10.1371/journal.pone.0221221.g006>

Table 3. Photocatalytic performance of magnetic photocatalysts after reuse.

| Catalyst or reaction system | Pollutants | Irradiation | Removal efficiency | | Reuse | Reaction Time | Reference |
|---|-----------------|---------------------|--------------------|---------|-------|---------------|-----------|
| | | | Fresh | Final | | | |
| Ni-Cu-Zn Ferrite@SiO ₂ @TiO ₂ @Ag | Methylene blue | Simulated sunlight | 87.8% | 46.2% | 5 | 6 h | [23] |
| TiO ₂ -FeZ and H ₂ O ₂ | Diclofenac | Simulated sunlight | ac. 89% | ac. 77% | 5 | 60 min | [62] |
| Ce/TiO ₂ /NiFe ₂ O ₄ /diatomite | Oxytetracycline | Visible light | 98.0% | 96.1% | 6 | 4 h | [40] |
| Fe ₃ O ₄ @SiO ₂ @TiO ₂ /Pd-Ag | Rhodamine B | UV irradiation | 96.1% | 84.0% | 6 | 40 min | [44] |
| Fe ₃ O ₄ @SiO ₂ @TiO ₂ /Pd | Rhodamine B | UV irradiation | 84.0% | 77.0% | 5 | 40 min | [44] |
| Fe ₃ O ₄ @C@CdS | Rhodamine B | Visible light | ac. 95% | ac. 86% | 6 | 50 min | [63] |
| Fe ₃ O ₄ @TiO ₂ | Rhodamine B | UV irradiation | ac. 80% | ac. 74% | 6 | - | [64] |
| TiO ₂ /montmorillonite/Fe ₃ O ₄ | Methylene blue | UV irradiation | 94.0% | 90.0% | 6 | 80 min | [21] |
| γ-Fe ₂ O ₃ @SiO ₂ @TiO ₂ -Ag | Methyl orange | UV irradiation | 84.5% | 82.0% | 18 | 60 min | [65] |
| ZnFe ₂ O ₄ /SrFe ₁₂ O ₁₉ | Methylene blue | UV-vis. irradiation | 96.6% | 70.6% | 5 | 60 min | [66] |
| Carbon-nanotubes/Fe ₃ O ₄ -ZnO | Methyl orange | UV irradiation | ac. 100% | ac. 90% | 2 | 45 min | [67] |
| Fe ₃ O ₄ @C@Cu ₂ O | Rhodamine B | Visible light | ac. 100% | ac. 95% | 6 | - | [68] |
| Barium-ferrite/SiO ₂ /TiO ₂ | Procion red | UV irradiation | ac. 60% | ac. 62% | 3 | 80 min | [69] |
| Heat-treated-BF/SiO ₂ /TiO ₂ | Procion red | UV irradiation | ac. 80% | ac. 80% | 3 | 80 min | [69] |
| Ag-TiO ₂ /SiO ₂ /Fe ₃ O ₄ | Orange II | UV irradiation | ac. 90% | ac. 80% | 3 | 20 min | [70] |
| Fe _x O _y /TiO ₂ -0.5 | R6G | UV irradiation | 45.0% | 98.4% | 5 | 6 h | This work |
| Fe _x O _y /TiO ₂ -0.35 | R6G | UV irradiation | 61.6% | 98.5% | 5 | 6 h | This work |
| Fe _x O _y @TiO ₂ -0.5 | R6G | UV irradiation | 67.4% | 97.3% | 5 | 6 h | This work |
| Fe _x O _y @TiO ₂ -0.35 | R6G | UV irradiation | 75.9% | 98.3% | 5 | 6 h | This work |

<https://doi.org/10.1371/journal.pone.0221221.t003>

time and chemical consumption by one-step facile synthesis. More studies can be introduced from this basis to target other objectives. For instance, iron-composing was reported to extend the excitation wavelength of TiO₂ nanophotocatalysts [60] or improve their photocatalytic efficiency [61], and the magnetism of iron-composing TiO₂ nanophotocatalysts can be altered by synthesis modification. Accordingly, our one-step facile synthesis of magnetic-TiO₂-nanophotocatalysts with high iron-composing ratio provides opportunities for synthesizing similar magnetic-TiO₂-nanocomposites with new features for further industrial applications.

4. Conclusion

In the present study, magnetic-TiO₂-nanocomposites with high iron-composing g ratio were prepared by a one-step coprecipitation method without any pre-synthesized precursor. Comparing to conventional two-step synthesized TiO₂-coating magnetic-nanocomposites with MNPs as precursor, we successfully decreased the synthesis time from 165 minutes to 75 minutes. Our results also proved that one-step synthesised magnetic-TiO₂-nanocomposites had satisfied R6G adsorption capability, photodegradation efficiency and photodegradation rate constant. The photocatalytic performance was dependent on Fe/Ti atomic ratio, and Fe_xO_y/TiO₂-0.35 was the most feasible nanophotocatalysts for industrial application. With facile synthesis process, comparable photocatalytic capability, acceptable viability of magnetic separation and satisfactory reusability, this synthesis method provides an alternative approach to prepare magnetic-TiO₂-nanophotocatalysts feasible for industrial practices.

Supporting information

S1 Table. Parameters for synthesizing magnetic-TiO₂-nanocomposites.

(DOCX)

S2 Table. Fe/Ti ratio of synthesizing magnetic-TiO₂-nanocomposites calculated by EDS results.

(DOCX)

S1 Fig. Photographs of synthesizing and harvesting the synthesized magnetic-TiO₂-nanocomposites.

(DOCX)

S2 Fig. TEM images of (A) Fe_xO_y/TiO₂-0.5, (B) Fe_xO_y/TiO₂-0.35 (C) Fe_xO_y@TiO₂-0.5 and (D) Fe_xO_y@TiO₂-0.35. Scale bar: 100 nm.

(DOCX)

S3 Fig. Energy dispersive spectroscopy (EDS) pattern of synthesized magnetic-TiO₂-nanocomposites. (A) Fe_xO_y/TiO₂-0.5, (B) Fe_xO_y/TiO₂-0.35 (C) Fe_xO_y@TiO₂-0.5 and (D) Fe_xO_y@TiO₂-0.35.

(DOCX)

S4 Fig. R6G adsorption kinetics on the synthesized magnetic-TiO₂-nanocomposites. (A) 1 mg/L, (B) 5 mg/L, (C) 10 mg/L, (D) 15 mg/L, (E) 20 mg/L, (F) 25 mg/L. Experimental conditions: magnetic-TiO₂-nanocomposites concentration, 0.4 g/L; pH, 7.0. Different small letters after each line indicate significant difference (Duncan's test, $p < 0.05$) among treatments

($n = 3$).

(DOCX)

S5 Fig. Impacts of pH on R6G adsorption on the synthesized magnetic-TiO₂-nanocomposites. Experimental conditions: initial magnetic-TiO₂-nanocomposite concentration, 0.4 g/L;

initial R6G concentration, 10 mg/L. Different small letters indicate significant difference (Duncan's test, $p < 0.05$) among treatments ($n = 3$).
(DOCX)

S6 Fig. R6G declining curves of the synthesized magnetic-TiO₂-nanocomposites without UV-irradiation. (A) pH = 3.0, (B) pH = 7.0, (C) pH = 10.0. Experimental conditions: initial magnetic-TiO₂-nanocomposites concentration, 0.4 g/L; initial R6G concentration, 10 mg/L. Different small letters after each line indicate significant difference (Duncan's test, $p < 0.05$) among treatments ($n = 3$).
(DOCX)

S7 Fig. Impacts of irradiation wavelength on the R6G photocatalytic degradation of the synthesized magnetic-TiO₂-nanocomposites. (A) 460 nm, (B) 540 nm. Different small letters after each line indicate significant difference (Duncan's test, $p < 0.05$) among treatments ($n = 3$).
(DOCX)

S8 Fig. Percentage of R6G loss during the photocatalysis process. The number in x-axis (0.2, 0.4 and 0.8) indicates the concentration of the synthesized magnetic-TiO₂-nanocomposites (mg/L), A refers to Fe_xO_y/TiO₂-0.5, B refers to Fe_xO_y/TiO₂-0.35, C refers to Fe_xO_y@TiO₂-0.5, and D refers to Fe_xO_y@TiO₂-0.35, respectively.
(DOCX)

S9 Fig. Effects of magnetic-TiO₂-nanocomposite concentration on R6G photodegradation kinetics. (A) Fe_xO_y/TiO₂-0.5, (B) Fe_xO_y/TiO₂-0.35, (C) Fe_xO_y@TiO₂-0.5 and (D) Fe_xO_y@TiO₂-0.35. Different small letters after each line indicate significant difference (Duncan's test, $p < 0.05$) among treatments ($n = 3$).
(DOCX)

Author Contributions

Conceptualization: Dayi Zhang.

Data curation: En Xie, Lei Zheng, Junfeng Dou.

Formal analysis: En Xie, Yingying Wang.

Writing – original draft: En Xie, Xinyang Li, Dayi Zhang.

Writing – review & editing: Aizhong Ding, Dayi Zhang.

References

1. Marien CBD, Cottineau T, Robert D, Drogui P (2016) TiO₂ Nanotube arrays: Influence of tube length on the photocatalytic degradation of Paraquat. *Applied Catalysis B Environmental* 194: 1–6.
2. Andreatti R, Caprio V, Insola A, Marotta R (1999) Advanced oxidation processes (AOP) for water purification and recovery. *Catalysis Today* 53: 51–59.
3. Mayorov AS, Gorbachev RV, Morozov SV, Britnell L, Jalil R, Ponomarenko LA, et al. (2011) Micrometer-scale ballistic transport in encapsulated graphene at room temperature. *Nano Letters* 11: 2396–2399. <https://doi.org/10.1021/nl200758b> PMID: 21574627
4. Hoffmann MR, Martin ST, Choi W, Bahnemann DW (1995) Environmental Applications of Semiconductor Photocatalysis. *Chemical Reviews* 95: 69–96.
5. Yao H, Fan M, Wang Y, Luo G, Fei W (2015) Magnetic titanium dioxide based nanomaterials: synthesis, characteristics, and photocatalytic application in pollutant degradation. *Journal of Materials Chemistry A* 3: 17511–17524.

6. Adán C, Bahamonde A, Martínez-Arias A, Fernández-García M, Pérez-Estrada LA, Malato S (2007) Solar light assisted photodegradation of ethidium bromide over titania-based catalysts. *Catalysis Today* 129: 79–85.
7. Jeng MJ, Wung YL, Chang LB, Chow L (2013) Particle size effects of TiO₂ layers on the solar efficiency. *International Journal of Photoenergy* 2013: 10510–10514.
8. Thao TL, Dang TT, Khanitchaidecha W, Channei D, Nakaruk A (2017) Photocatalytic Degradation of Organic Dye under UV-A Irradiation Using TiO₂-Vetiver Multifunctional Nano Particles. *Materials* 10: E122. <https://doi.org/10.3390/ma10020122> PMID: 28772482
9. Saliu Oluwaseyi D, Olatunji Gabriel A, Yakubu A, Arowona Mariam T, Mohammed Aminat A (2017) Catalytic crosslinking of a regenerated hydrophobic benzylated cellulose and nano TiO₂ composite for enhanced oil absorbency. *e-Polymers* 17: 295–302.
10. Seaton A, Tran L, Aitken R, Donaldson K (2010) Nanoparticles, human health hazard and regulation. *Journal of the Royal Society* 7: S119–S129.
11. Shan AY, Ghazi TIM, Rashid SA (2010) Immobilisation of titanium dioxide onto supporting materials in heterogeneous photocatalysis: A review. *Applied Catalysis A: General* 389: 1–8.
12. Yeganeh M, Shahtahmasebi N, Kompany A, Karimipour M, Razavi F, Nasralla NHS, et al. (2017) The magnetic characterization of Fe doped TiO₂ semiconducting oxide nanoparticles synthesized by sol-gel method. *Physica B: Condensed Matter* 511: 89–98.
13. Ai L, Huang H, Chen Z, Wei X, Jiang J (2010) Activated carbon/CoFe₃O₄ composites: Facile synthesis, magnetic performance and their potential application for the removal of malachite green from water. *Chemical Engineering Journal* 156: 243–249.
14. Zhang DY, Berry JP, Zhu D, Wang Y, Chen Y, Jiang B, et al. (2015) Magnetic nanoparticle-mediated isolation of functional bacteria in a complex microbial community. *ISME Journal* 9: 603–614. <https://doi.org/10.1038/ismej.2014.161> PMID: 25191996
15. Iranmanesh M, Hulliger J (2017) Magnetic separation: its application in mining, waste purification, medicine, biochemistry and chemistry. *Chemical Society Reviews* 46: 5925–5934. <https://doi.org/10.1039/c7cs00230k> PMID: 28730213
16. Yavuz CT, Mayo JT, Yu WW, Prakash A, Falkner JC, Yean S, et al. (2006) Low-Field Magnetic Separation of Monodisperse Fe₃O₄ Nanocrystals. *Science* 314: 964–967. <https://doi.org/10.1126/science.1131475> PMID: 17095696
17. Jing Y, Moore LR, Williams PS, Chalmers JJ, Farag SS, Bolwell B, et al. (2007) Blood progenitor cell separation from clinical leukapheresis product by magnetic nanoparticle binding and magnetophoresis. *Biotechnology and Bioengineering* 96: 1139–1154. <https://doi.org/10.1002/bit.21202> PMID: 17009321
18. Gu H, Xu K, Xu C, Xu B (2006) Biofunctional magnetic nanoparticles for protein separation and pathogen detection. *Chemical Communications*: 941–949. <https://doi.org/10.1039/b514130c> PMID: 16491171
19. Lin Z, Xu Y, Zhen Z, Fu Y, Liu Y, Li W, et al. (2015) Application and reactivation of magnetic nanoparticles in *Microcystis aeruginosa* harvesting. *Bioresource Technology* 190: 82–88. <https://doi.org/10.1016/j.biortech.2015.04.068> PMID: 25935387
20. Wang XZ, Zhao XH, Li HB, Jia JL, Liu Y, Ejenavi O, et al. (2016) Separating and characterizing functional alkane degraders from crude-oil-contaminated sites via magnetic nanoparticle-mediated isolation. *Research in Microbiology* 167: 731–744. <https://doi.org/10.1016/j.resmic.2016.07.004> PMID: 27475037
21. Zhang P, Mo Z, Han L, Zhu X, Bo W, Zhang C (2014) Preparation and Photocatalytic Performance of Magnetic TiO₂/Montmorillonite/Fe₃O₄ Nanocomposites. *Industrial & Engineering Chemistry Research* 53: 8057–8061.
22. Chen Z, Ma Y, Geng B, Wang M, Sun X (2017) Photocatalytic performance and magnetic separation of TiO₂-functionalized γ -Fe₂O₃, Fe, and Fe/Fe₂O₃ magnetic particles. *Journal of Alloys and Compounds* 700: 113–121.
23. Chen C, Jaihindh D, Hu S, Fu Y (2017) Magnetic recyclable photocatalysts of Ni-Cu-Zn ferrite@SiO₂@-TiO₂@Ag and their photocatalytic activities. *Journal of Photochemistry and Photobiology A: Chemistry* 334: 74–85.
24. Ali T, Tripathi P, Ameer A, Waseem R, Arham SA, Ateeq A, et al. (2017) Photocatalytic performance of Fe-doped TiO₂ nanoparticles under visible-light irradiation. *Materials Research Express* 4: 015022.
25. Wang Q, Yang C, Zhang G, Hu L, Wang P (2017) Photocatalytic Fe-doped TiO₂/PSF composite UF membranes: Characterization and performance on BPA removal under visible-light irradiation. *Chemical Engineering Journal* 319: 39–47.
26. Răileanu M, Crișan M, Nițoi I, Ianculescu A, Oancea P, Crișan D, et al. (2013) TiO₂-based Nanomaterials with Photocatalytic Properties for the Advanced Degradation of Xenobiotic Compounds from Water. A Literature Survey. *Water, Air, & Soil Pollution* 224: 1548.

27. Choi W, Termin A, Hoffmann MR (1994) The Role of Metal Ion Dopants in Quantum-Sized TiO₂: Correlation between Photoreactivity and Charge Carrier Recombination Dynamics. *Journal of Physical Chemistry* 98: 13669–13679.
28. Zhao B, Mele G, Pio I, Li J, Palmisano L, Vasapollo G (2010) Degradation of 4-nitrophenol (4-NP) using Fe-TiO₂ as a heterogeneous photo-Fenton catalyst. *Journal of Hazardous Materials* 176: 569–574. <https://doi.org/10.1016/j.jhazmat.2009.11.066> PMID: 20004519
29. Ganesh I, Kumar PP, Gupta AK, Sekhar PSC (2012) Preparation and characterization of Fe-doped TiO₂ powders for solar light response and photocatalytic applications. *Processing & Application of Ceramics* 6: 21–36.
30. Zhang D, Fakhrullin RF, Özmen M, Wang H, Wang J, Paunov VN, et al. (2011) Functionalization of whole-cell bacterial reporters with magnetic nanoparticles. *Microbial Biotechnology* 4: 89–97. <https://doi.org/10.1111/j.1751-7915.2010.00228.x> PMID: 21255376
31. Zhao X, Li H, Ding A, Zhou G, Sun Y, Zhang D (2016) Preparing and characterizing Fe₃O₄@cellulose nanocomposites for effective isolation of cellulose-decomposing microorganisms. *Materials Letters* 163: 154–157.
32. Wang X, Zhao X, Li H, Jia J, Liu Y, Ejenavi O, et al. (2016) Separating and characterizing functional alkane degraders from crude-oil-contaminated sites via magnetic nanoparticle-mediated isolation. *Research in Microbiology* 167: 731–744. <https://doi.org/10.1016/j.resmic.2016.07.004> PMID: 27475037
33. Ambrus Z, Balázs N, Alapi T, Wittmann G, Sipos P, Dombi A, et al. (2008) Synthesis, structure and photocatalytic properties of Fe(III)-doped TiO₂ prepared from TiCl₃. *Applied Catalysis B: Environmental* 81: 27–37.
34. Muthukumar T, Gnanaprakash G, Philip J (2012) Synthesis of Stable Magnetic Nanofluids of Different Particle Sizes. *Journal of Nanofluids* 1: 85–92.
35. Zhang L, Wu Z, Chen L, Zhang L, Li X, Xu H, et al. (2016) Preparation of magnetic Fe₃O₄/TiO₂/Ag composite microspheres with enhanced photocatalytic activity. *Solid State Sciences* 52: 42–48.
36. Yamashita T, Hayes P (2008) Analysis of XPS spectra of Fe²⁺ and Fe³⁺ ions in oxide materials. *Applied Surface Science* 254: 2441–2449.
37. Bhowmick S, Chakraborty S, Mondal P, Van Renterghem W, Van den Berghe S, Roman-Ross G, et al. (2014) Montmorillonite-supported nanoscale zero-valent iron for removal of arsenic from aqueous solution: Kinetics and mechanism. *Chemical Engineering Journal* 243: 14–23.
38. Iram M, Guo C, Guan Y, Ishfaq A, Liu H (2010) Adsorption and magnetic removal of neutral red dye from aqueous solution using Fe₃O₄ hollow nanospheres. *Journal of Hazardous Materials* 181: 1039–1050. <https://doi.org/10.1016/j.jhazmat.2010.05.119> PMID: 20566240
39. Pandey SK, Choudhary RJ (2011) Effect of non-magnetic impurities on the magnetic states of anatase TiO₂. *Journal of Physics Condensed Matter* 23: 276005. <https://doi.org/10.1088/0953-8984/23/27/276005> PMID: 21690657
40. Yan C, Kuren L (2017) Magnetic Ce-doped TiO₂/NiFe₂O₄/diatomite ternary composite: Enhanced visible-light-driven photocatalytic performance. *Powder Technology* 313: 44–53.
41. Habibi-Yangjeh A, Shekofteh-Gohari M (2016) Fe₃O₄/ZnO/Ag₃VO₄/AgI nanocomposites: Quaternary magnetic photocatalysts with excellent activity in degradation of water pollutants under visible light. *Separation and Purification Technology* 166: 63–72.
42. Zielińska-Jurek A, Bielani Z, Wysocka I, Strychalska J, Janczarek M, Klimczuk T (2017) Magnetic semiconductor photocatalysts for the degradation of recalcitrant chemicals from flow back water. *Journal of Environmental Management* 195: 157–165. <https://doi.org/10.1016/j.jenvman.2016.06.056> PMID: 27394084
43. He Z, Hong T, Chen J, Song S (2012) A magnetic TiO₂ photocatalyst doped with iodine for organic pollutant degradation. *Separation and Purification Technology* 96: 50–57.
44. Khojasteh H, Salavati-Niasari M, Mazhari M-P, Hamadani M (2016) Preparation and characterization of Fe₃O₄@SiO₂@TiO₂@Pd and Fe₃O₄@SiO₂@TiO₂@Pd-Ag nanocomposites and their utilization in enhanced degradation systems and rapid magnetic separation. *RSC Advances* 6: 78043–78052.
45. Chen S, Zhang Y, Han W, Wellburn D, Liang J, Liu C (2013) Synthesis and magnetic properties of Fe₂O₃-TiO₂ nano-composite particles using pulsed laser gas phase evaporation–liquid phase collecting method. *Applied Surface Science* 283: 422–429.
46. Gondal MA, Chang XF, Yamani ZH (2010) UV-light induced photocatalytic decolorization of Rhodamine 6G molecules over BiOCl from aqueous solution. *Chemical Engineering Journal* 165: 250–257.
47. Yang S, Chen Y, Zheng J, Cui Y (2007) Enhanced photocatalytic activity of TiO₂ by surface fluorination in degradation of organic cationic compound. *Journal of Environmental Sciences* 19: 86–89.
48. Khalyavka TA, Kapinus EI, Viktorova TI, Tsyba NN (2009) Adsorption and photocatalytic properties of nanodimensional titanium–zinc oxide composites. *Theoretical and Experimental Chemistry* 45: 234.

49. Gomathi DL, Narasimha MB, Girish KS (2009) Heterogeneous photo catalytic degradation of anionic and cationic dyes over TiO₂ and TiO₂ doped with Mo⁶⁺ ions under solar light: Correlation of dye structure and its adsorptive tendency on the degradation rate. *Chemosphere* 76: 1163–1166. <https://doi.org/10.1016/j.chemosphere.2009.04.005> PMID: 19439341
50. Chiou C-H, Wu C, Juang R-S (2008) Influence of operating parameters on photocatalytic degradation of phenol in UV/TiO₂ process. *Chemical Engineering Journal* 139: 322–329.
51. Kong L, Lu X, Bian X, Zhang W, Wang C (2014) Constructing Carbon-Coated Fe₃O₄ Microspheres as Antiacid and Magnetic Support for Palladium Nanoparticles for Catalytic Applications. *ACS applied materials & interfaces* 3: 35–42.
52. Rajoriya S, Bargole S, Saharan VK (2017) Degradation of a cationic dye (Rhodamine 6G) using hydrodynamic cavitation coupled with other oxidative agents: Reaction mechanism and pathway. *Ultrasonics sonochemistry* 34: 183–194. <https://doi.org/10.1016/j.ultsonch.2016.05.028> PMID: 27773234
53. Asiri AM, Al-Amoudi MS, Al-Talhi TA, Al-Talhi AD (2011) Photodegradation of Rhodamine 6G and phenol red by nanosized TiO₂ under solar irradiation. *Journal of Saudi Chemical Society* 15: 121–128.
54. Chakhari W, Ben Naceur J, Ben Taieb S, Ben Assaker I, Chtourou R (2017) Fe-doped TiO₂ nanorods with enhanced electrochemical properties as efficient photoanode materials. *Journal of Alloys and Compounds* 708: 862–870.
55. Yu J, Xiang Q, Zhou M (2009) Preparation, characterization and visible-light-driven photocatalytic activity of Fe-doped titania nanorods and first-principles study for electronic structures. *Applied Catalysis B: Environmental* 90: 595–602.
56. Chen D, Ray AK (1998) Photodegradation kinetics of 4-nitrophenol in TiO₂ suspension. *Water Research* 32: 3223–3234.
57. Guo J, Al-Dahhan M (2006) Activity and stability of iron-containing pillared clay catalysts for wet air oxidation of phenol. *Applied Catalysis A: General* 299: 175–184.
58. Gao Y, Zhang Z, Li S, Jin L, Yao L, Li Y, et al. (2016) Insights into the mechanism of heterogeneous activation of persulfate with a clay/iron-based catalyst under visible LED light irradiation. *Applied Catalysis B: Environmental* 185: 22–30.
59. Thompson TL, Yates J, John T. (2006) Surface Science Studies of the Photoactivation of TiO₂-New Photochemical Processes. *Chemical Reviews* 38: 4428–4453.
60. Huy BT, Jung DS, Kim Phuong NT, Lee YI (2017) Enhanced photodegradation of 2,4-dichlorophenoxyacetic acid using a novel TiO₂@MgFe₂O₄ core@shell structure. *Chemosphere* 184: 849–856. <https://doi.org/10.1016/j.chemosphere.2017.06.069> PMID: 28646767
61. Pal NK, Kryschi C (2016) Improved photocatalytic activity of gold decorated differently doped TiO₂ nanoparticles: A comparative study. *Chemosphere* 144: 1655–1664. <https://doi.org/10.1016/j.chemosphere.2015.10.060> PMID: 26519796
62. Salaeh S, Kovacic M, Kosir D, Kusic H, Lavrencic Stangar U, Dionysiou DD, et al. (2017) Reuse of TiO₂-based catalyst for solar driven water treatment; thermal and chemical reactivation. *Journal of Photochemistry and Photobiology A: Chemistry* 333: 117–129.
63. Li D, Xie J, Zhang Y, Qiao R, Li S, Li Z (2015) Convenient synthesis of magnetically recyclable Fe₃O₄@C@CdS photocatalysts by depositing CdS nanocrystals on carbonized ferrocene. *Journal of Alloys and Compounds* 646: 978–982.
64. Xin T, Ma M, Zhang H, Gu J, Wang S, Liu M, et al. (2014) A facile approach for the synthesis of magnetic separable Fe₃O₄@TiO₂, core-shell nanocomposites as highly recyclable photocatalysts. *Applied Surface Science* 288: 51–59.
65. Cui B, Peng H, Xia H, Guo X, Guo H (2013) Magnetically recoverable core-shell nanocomposites γ-Fe₂O₃@SiO₂@TiO₂-Ag with enhanced photocatalytic activity and antibacterial activity. *Separation and Purification Technology* 103: 251–257.
66. Xie T, Xu L, Liu C, Wang Y (2013) Magnetic composite ZnFe₂O₄/SrFe₁₂O₁₉: Preparation, characterization, and photocatalytic activity under visible light. *Applied Surface Science* 273: 684–691.
67. Sui J, Li J, Li Z, Cai W (2012) Synthesis and characterization of one-dimensional magnetic photocatalytic CNTs/Fe₃O₄-ZnO nanohybrids. *Materials Chemistry and Physics* 134: 229–234.
68. Li S, Huang F, Wang Y, Shen Y, Qiu L, Xie A, et al. (2011) Magnetic Fe₃O₄@C@Cu₂O composites with bean-like core/shell nanostructures: synthesis, properties and application in recyclable photocatalytic degradation of dye pollutants. *Journal of Materials Chemistry* 21: 7459–7466.
69. Lee S-w, Drwiega J, Mazyck D, Wu C-Y, Sigmund WM (2006) Synthesis and characterization of hard magnetic composite photocatalyst—Barium ferrite/silica/titania. *Materials Chemistry and Physics* 96: 483–488.
70. Xu M, Bao S, Zhang X (2005) Enhanced photocatalytic activity of magnetic TiO₂ photocatalyst by silver deposition. *Materials Letters* 59: 2194–2198.